J. Mol. Biol. (1995) 251, 282–296

JMB

Crystal Structure of Reduced Bovine Erythrocyte Superoxide Dismutase at 1.9 Å Resolution

Wojciech R. Rypniewski[1]*, Stefano Mangani[2], Bruno Bruni[3] Pier Luigi Orioli[3], Marco Casati[3] and Keith S. Wilson[1]

[1]*European Molecular Biology Laboratory (EMBL) c/o DESY, Notkestrasse 85 22603 Hamburg, Germany*

[2]*Department of Chemistry University of Siena, Pian dei Mantellini 44, 53100 Siena Italy*

[3]*Department of Chemistry University of Florence via G. Capponi 7 50121 Firence, Italy*

**Corresponding author*

Cu,Zn superoxide dismutase was investigated crystallographically in the reduced form. Co-ordinate errors were estimated by comparing two independently refined models, based on two different data sets. This gave a detailed error estimation as opposed to the standard σ_A and Luzzati plots, which estimate only the overall error. The high quality of the final model, obtained after scaling together the two data sets, combined with the error estimates allowed a detailed analysis of the protein and solvent structures. An automatic procedure for building and refining solvent structure was tested and found to give reproducible results. Contrary to results obtained from spectroscopic studies, the co-ordination of the metal ions in the catalytic site is preserved in the crystal structure of the reduced enzyme, as compared with the crystal structure of the oxidised form. Analysis of the solvent reveals a well-defined chain of closely packed, hydrogen-bonded water molecules filling the active site groove. This structural feature could serve as a hydrogen bond relay for efficient delivery of protons to the active centre. Analysis of electron density suggests that Glu119 is covalently modified. The modification, if originated *in vivo*, could have a role in the catalytic mechanism and could affect the overall electrostatic field in the active site. There are significant differences between the active sites of the two crystallographically independent monomers. They are explained in terms of local differences in the crystal environment.

Keywords: superoxide dismutase; X-ray; structure; copper; zinc

Introduction

Cu,Zn superoxide dismutase (SOD) is a dimeric enzyme of molecular mass 32,000 daltons, which catalyses the dismutation of the superoxide anion to oxygen and hydrogen peroxide (Fridovich, 1975). The protein contains Cu^{2+} and Zn^{2+} in the active site and the catalytically active Cu^{2+} is cyclically reduced and oxidised during the process. The reaction mechanism proceeds in two steps (Klug *et al.*, 1972):

$$\text{E-Cu(II)} + O_2^- + H^+ \rightleftharpoons \text{EH-Cu(I)} + O_2$$

$$\text{EH-Cu(I)} + O_2^- + H^+ \rightleftharpoons \text{E-Cu(II)} + H_2O_2$$

$$2O_2^- + 2H^+ \rightleftharpoons O_2 + H_2O_2$$

The oxidised superoxide dismutase has been well characterised by X-ray studies of the bovine enzyme (Tainer *et al.*, 1982; Djinovic *et al.*, 1992) and by several physical methods (Bertini *et al.*, 1990; Rotilio *et al.*, 1971; Valentine & Pantoliano, 1981). It has been found that in the active site the copper ion is co-ordinated by the nitrogen atoms of four histidine residues and by a water molecule. One of the histidine residues (His61) bridges copper and zinc. Co-ordination of zinc is completed by two other histidine residues and an aspartate residue in a tetrahedral geometry.

For reduced SOD, containing Cu^+, UV/visible absorption spectroscopy (McAdam *et al.*, 1977), NMR (Bertini *et al.*, 1985, 1991; Azab *et al.*, 1992) and EXAFS data (Blackburn *et al.*, 1984) are available. The spectroscopic studies provide evidence for the breaking of the copper-nitrogen bond of the bridging histidine residue (His61) and simultaneous protonation of $N^{\varepsilon 2}$ of the same residue. In view of the lack of X-ray diffraction evidence, we decided to determine the crystal structure of the reduced enzyme. Our preliminary X-ray investigations (Banci *et al.*, 1994) revealed that, contrary to spectroscopic data, no major structural change took place upon reduction of the enzyme in crystalline form. The SOD crystals were obtained from solutions of the native enzyme treated with sodium dithionite under nitro-

Abbreviations used: SOD, Cu,Zn superoxide dismutase; EXAFS, extended X-ray absorption fine structure; EPR, electron paramagnetic resonance.

0022–2836/95/320282–15 $12.00/0

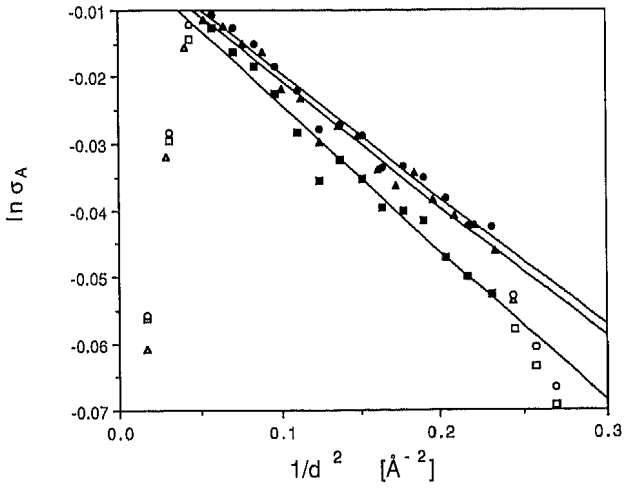

Figure 1. σ_A plot (Read, 1986) for SODr_1 (squares), SODr_2 (triangles) and final SODr model (circles). Data points not used in fitting the straight line are shown as void symbols.

gen atmosphere. The crystals were colourless and the EPR spectrum taken before and after data collection, was featureless. Comparable crystals of oxidised SOD showed EPR spectrum characteristic of copper (II). While these results confirmed that the enzyme was indeed reduced, we were surprised to find that in the crystal structure the co-ordination of the copper ion remains unchanged compared with the oxidised state. As this contradicts the spectroscopic results, we decided to repeat the experiment on another crystal. The second experiment confirmed our earlier results. His61 was clearly bound to the copper ion while the EPR spectra, again taken before and after data collection, confirmed that copper was reduced. The crystal remained colourless throughout data collection and subsequent EPR spectroscopy.

As it became apparent that any change in the crystal structure upon reduction would be small, we undertook a detailed analysis attempting to make the best use of the high quality of our X-ray data. We decided initially not to merge the two data sets but to refine two models independently. Comparing the two models enabled us to obtain a much more detailed estimate of errors in atomic co-ordinates than would have been possible by traditional means (Luzzati, 1952; Read, 1986). Comparison of solvent structure enabled us to assess the reliability of the protocol for an automatic building and refinement of solvent. Finally, the two data sets were merged, giving a high-quality data set with twice the usual redundancy, and the refinement was completed.

† The standard deviation estimating the error in atomic positions was calculated as $\sqrt{\Sigma(d^2/2)}$ where d is the distance between the corresponding pairs of atoms. The summation is over all relevant atoms. This formulation should be distinguished from $\sqrt{\Sigma d^2}$ commonly used in estimating the difference ("distance") between two different structures.

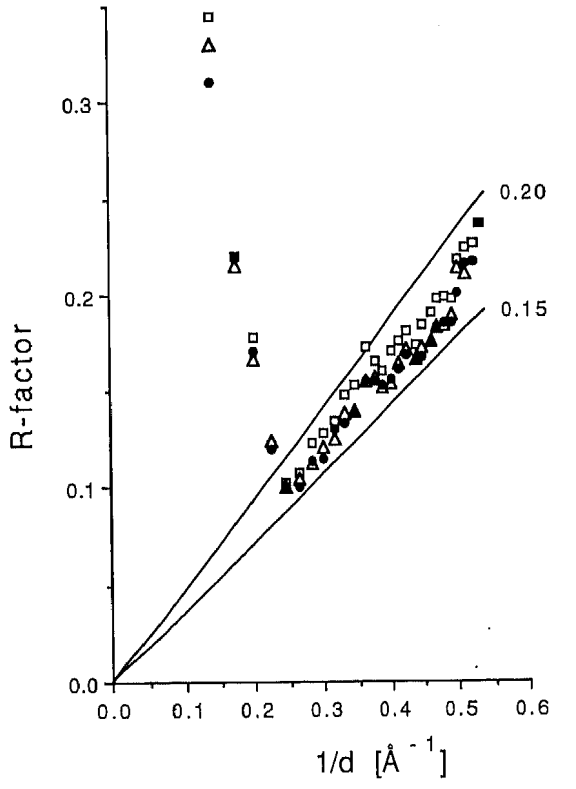

Figure 2. Plot of the R-factor as a function of inverse resolution for SODr_1 (squares), SODr_2 (triangles) and final SODr model (filled circles). The straight lines show the theoretical dependence of the R-factor on resolution for the mean co-ordinate errors shown on the right (Luzzati, 1952).

Results and Discussion

Assessing co-ordinate error by traditional methods

The mean co-ordinate error estimated from σ_A plots (Figure 1) is 0.18 Å and 0.17 Å for the SODr_1 and SODr_2, models respectively. For the final model it is 0.17 Å, similar to SODr_2. Very similar values can be derived from the Luzzati plot (Figure 2). Based on the plots, the accuracy of the final model can be judged to be slightly better than either SODr_1 of SODr_2. Although the differences are small, especially when compared with SODr_2, the outliers for the final model deviate less from the theoretical straight line.

Estimation of errors by comparing the two independently refined models

The two models were superimposed by least-squares minimisation of positions for all protein atoms. This resulted in a small rotation (Eulerian angles $\alpha = 2.4°$, $\beta = 0.3°$, $\gamma = -2.4°$) and translation ($\Delta x = -0.21$ Å, $\Delta y = 0.06$ Å, $\Delta z = 0.13$ Å) of SOD_2 relative to SOD_1. The largest difference is along the x-axis and can partly be explained by differences in cell parameters, which were largest along the a-axis. The r.m.s. deviation in position† for protein atoms

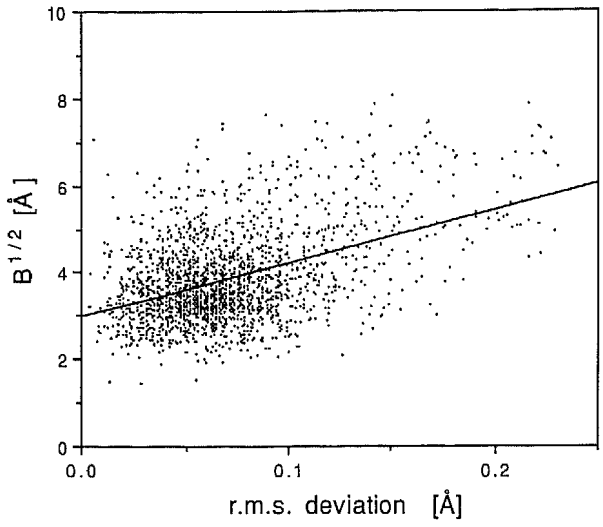

Figure 3. Estimated root-mean-square error in co-ordinates for all protein atoms in the final SODr model plotted against the square-root of atomic temperature factor. The r.m.s. error was derived by pairwise comparison of atomic co-ordinates from the two independently refined SODr models (see the text). Temperature factors were averaged for each pair of atoms. The linear correlation coefficient is 0.4.

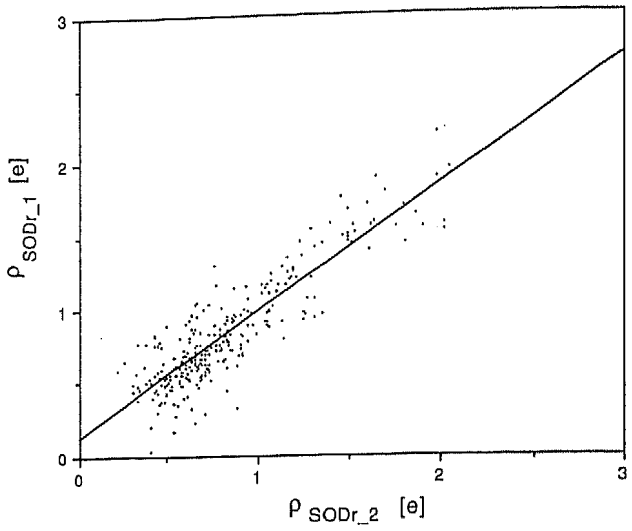

Figure 4. A comparison of solvent electron density in SODr_1 (vertical axis) against SODr_2 (horizontal axis) for all 271 solvent sites independently predicted (see the text for criteria) in both models.

between SODr_1 and SODr_2 was calculated and 38 atoms were found to deviate by more than 3σ and were omitted from the model. They were all poorly ordered side-chain atoms, except for N-terminal amide groups from both subunits. In the final model all protein atoms had positional deviations less than 3σ from the mean deviation. The final r.m.s. deviation was 0.08 Å for all protein atoms, 0.07 Å for the main-chain atoms and 0.09 Å for the side-chains. This is considerably less than the estimated error from σ_A and Luzzati plots. The difference is probably due to the fact that σ_A and Luzzati plots estimate the error for all atoms, whereas in the above comparison of the two models only the ordered protein atoms were used. The solvent atoms will be analysed later. Using the above value of 0.08 Å for the standard deviation in atomic position for the protein atoms, we obtain 0.11 Å as the standard deviation of the distance between pairs of atoms†. It should be borne in mind that the true value will be more for poorly ordered side-chain atoms and less for well-ordered main-chain and side-chain atoms.

In conclusion, while the σ_A and Luzzati plots are commonly used to estimate the average error in atomic co-ordinates they are based on theoretical considerations. Comparing two independently refined models allows an empirical estimation of the errors. It also allows us to estimate errors for individual atoms or groups of atoms. It can be used in cases where full-matrix or block-matrix refinement is not feasible.

The plot of the positional r.m.s. deviations of the individual protein atoms against the square-root of temperature factors, averaged for each atom (Figure 3), shows a weakly linear dependence, with correlation coefficient 0.40. Extrapolation to the origin gives a temperature factor of approximately 9 Å^2 for a perfectly fitting average atom.

The average *B*-values for protein atoms in SODr_1 and SODr_2 were 15.7 Å^2 and 15.1 Å^2 reflecting the slightly higher quality of the second data set. The r.m.s deviation in temperature factors for all protein atoms, calculated by comparing the two models, was 1.6 Å^2. This decreased slightly to 1.5 Å^2 when the *B*-factors of the second model were adjusted to make the mean *B*-values equal for both models.

The automatic refinement procedure of ARP (Lamzin & Wilson, 1993) gave 299 water molecules for SODr_1 and 349 for SODr_2. Comparison of the two models, superimposed on the protein atoms, gave 271 solvent sites with water molecules occurring within 1.5 Å of each other. This is 90% of the 299 possible sites. The r.m.s. deviation in position, calculated based on the distance between water molecules within each pair, was 0.30 Å. Only four water molecule sites had r.m.s. deviations slightly greater than 3σ. A plot of electron density at the centre of one water molecule against the density at the other, for each of the 271 pairs, shows a good linear dependence, with linear correlation coefficient of 0.88, and a straight line passing near the origin (Figure 4). A plot of electron density at the water molecule for SODr_1 (Figure 5) against the r.m.s value, for each pair, shows that low r.m.s values are in general associated with high electron density and *vice versa*, but also many sites with low density have low r.m.s. values. This makes it impossible to define,

† $\sigma(dist) = \sqrt{\sigma^2(pos_1) + \sigma^2(pos_2)}$. In this case we take the mean estimated value for positional standard deviation for protein atoms. This gives $\sigma(dist) = \sqrt{2}\sigma(pos)$.

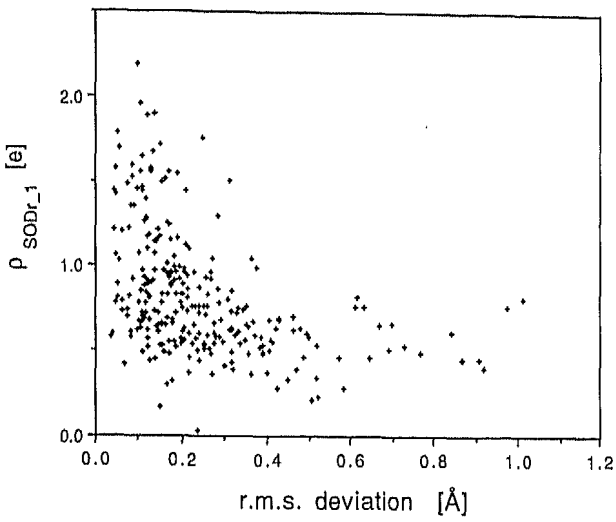

Figure 5. A plot of estimated r.m.s. error in co-ordinates for SODr_1 against the electron density at the atomic centre, for the corresponding 271 solvent sites independently found in both models. The plot for SODr_2 (not shown) is similar.

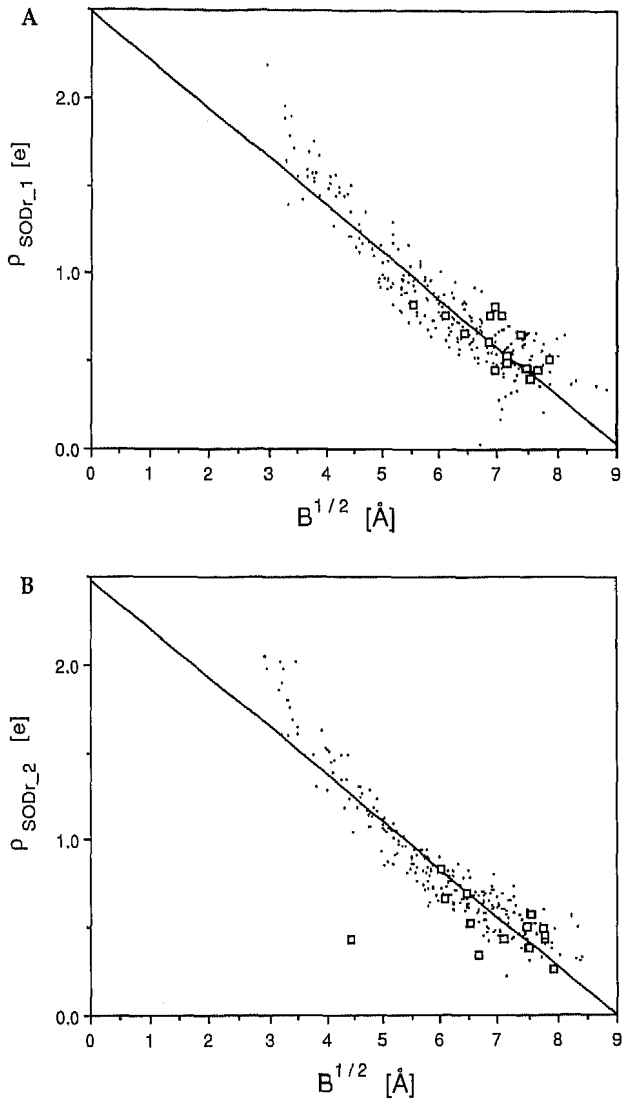

Figure 6. A plot of electron density at the atomic centre for (a) SODr_1 and (b) SODr_2 against the square-root of temperature factor, for the 271 solvent sites found by comparing the two models. Solvent molecules with estimated r.m.s. error in co-ordinates greater than three standard deviations are marked with squares. Standard deviation was estimated by comparing co-ordinates of all the 271 solvent molecules in the two models.

by means of this simple analysis, an overall significant threshold of electron density for defining new solvent molecules. The water molecules that have low density but are reproducibly obtained probably represent partially occupied solvent sites. Inspection of electron density confirms that many weak peaks in the solvent region are well defined spatially, are within hydrogen-bonding distances of protein or solvent atoms, appear persistently throughout refinement and, in this case, on maps derived from independently collected data sets. Refining such water molecules at full occupancy will result in overestimated temperature factors. When a low occupancy site is modelled by a fully occupied water molecule the resulting peak is broadened and flattened in the course of least-squares refinement to make the electron density near the centre of the atom comparable to the true density. This may result in distortions of the $(F_o - F_c)$ density map away from the centre of the atom. When a small, well-defined peak is subtracted from a much broader peak of similar maximum height, the resulting residual density on the $(F_o - F_c)$ density map may be higher in regions surrounding the peak seen on the $(3F_o - 2F_c)$ map than at its centre. As a result, such water molecules tend to drift during the refinement, away from their initial positions in the centre of the peak in the $(3F_o - 2F_c)$ map and are usually rejected. The ARP option of using real space refinement to optimise the position of the water molecules, based on the $(3F_o - 2F_c)$ map, is particularly useful in maintaining the position of low occupancy water molecules.

A plot of electron density at water positions, for the 271 sites, against the square-root of temperature factor (Figure 6) shows a strong linear dependence, with correlation coefficient 0.92 for both SODr_1 and SODr_2. In both cases, there is a systematic deviation from the straight line at high electron density and low temperature factors. In light of the above argument, it is likely that the deviation is in fact in the low-density, high B-values region, with many of the low-density sites being partially occupied, and a resulting overestimation of temperature factors.

While refining occupancy factors is not feasible in the absence of high-resolution data, it is reasonable to approximate a low-occupancy solvent site by a water molecule at full occupancy and elevated B-factor. But one must then expect that some water molecules will have higher temperature factors than would be expected if only fully occupied sites were present. Figure 6 also shows that even water mol-

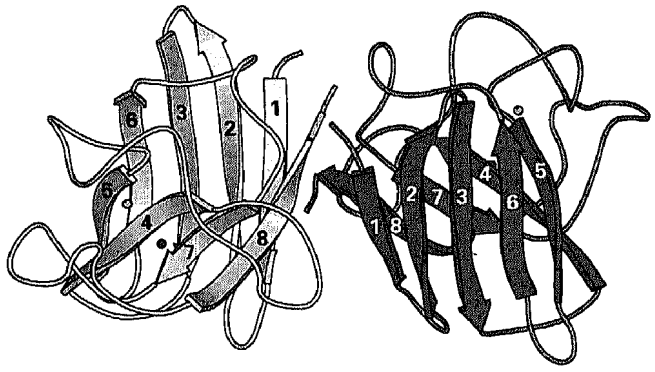

Figure 7. Ribbon diagram of the SODr dimer. The metal ions are drawn as spheres, copper (dark) and zinc (light). The left subunit shows the disposition of the active site, outside the β-barrel, adjacent to strands 4, 5 and 7, and flanked by two loops, between strands 4 and 5, and 7 and 8. The diagram was drawn with MOLSCRIPT (Kraulis, 1991).

ecules with relatively high estimated r.m.s. errors in position fall well within the overall distribution of electron density and *B*-factors. We conclude that the adopted procedure for automatic search and verification of solvent molecules is valid, although the final model should be verified by manual inspection of the electron density map. The distribution shown in Figure 6 also indicates that water molecules with *B*-factors of up to about 80 Å^2 should, in principle, be considered, provided they lie in significant electron density. ARP provides a convenient means for estimating statistically significant threshold in a difference electron density.

The final model

The SOD subunit can be described as a "split" β-barrel, with no direct hydrogen bonds between main-chain atoms of β-strands 5 and 6. Two extensive loops between strands 4 and 5, and strands 7 and 8, form part of the active site (Figures 7 and 8).

Average temperature factors for the final model were 14.7 Å^2 for main-chain atoms, 19.3 Å^2 for side-chains, 16.7 Å^2 for all protein atoms and 44.3 Å^2 for the solvent. The histogram of solvent *B*-factors (Figure 9) has several maxima giving some indication of the successive solvation shells around the protein. The average *B*-factor for the all atoms was 20.7 Å^2, in reasonable agreement with the value of 24.3 Å^2 obtained from the Wilson plot (see Figure 17). The difference is probably due to partially disordered solvent that was not included in the model.

The overall structure is similar to the oxidised, cobalt-substituted SOD (Djinovic *et al.* 1992). Least-squares minimisation using all C$^\alpha$ atoms gave r.m.s. deviation of 0.19 Å between the two structures. Only two residues, Gly128 and Asn129, deviated by more than 3 r.m.s. Both residues lie on the surface and have relatively high temperature factors, with expected co-ordinate errors larger than average. After omitting these residues the r.m.s. deviations decreased slightly to 0.18 Å.

Comparison of subunits A and B

Subunits A and B were superimposed by least-squares minimisation. Initial comparison using all C$^\alpha$ atoms gave r.m.s. deviation of 0.30 Å. After omitting residues 23 to 26, 100 and 128 to 130, with deviations greater than 3 r.m.s., the final superposition had a standard deviation of 0.19 Å (Figure 10). This is greater than the estimated experimental error of 0.11 Å and probably reflects differences due to different crystal environment of subunits A and B. There is a clear correlation between crystal contacts and the difference in co-ordinates between subunits A and B. The largest differences in co-ordinates are associated with crystal contacts. There are only two distinct regions of intermolecular contacts in SODr. One involves subunit A and its symmetry-related equivalent, the other involves subunit B and its symmetry-related equivalent. Table 1 represents the crystal contacts schematically. The contacts between subunits B are more extensive than between subunits A, with 25 intermolecular interactions shorter than 3.5 Å between subunits B and 13 interactions between subunits A. Both areas of contact involve similar regions of the molecular surface for subunits A and B but the details of the interactions are different. The crystal contacts in the region around residue 65 have the least effect on local co-ordinates, with differences of up to approximately 3σ of the experimental error estimate. This crystal contact is nearest to the active centre of the enzyme. The possible effects of this contact region on the water structure in the active site will be discussed below. The residues co-ordinating the metal ions can be superimposed well within the estimated experimental error. Intermolecular contacts also affect the temperature factors, particularly in the region around residue 130 in subunit B (Figure 11).

Catalytic centre

The co-ordination bond distances and angles in the metal centres for SODr_1, SODr_2, the final model and the corresponding oxidised, cobalt-substituted structure (Djinovic *et al.*, 1992) are shown in Table 2. Most of the differences between SODr_1 and SODr_2 are well within one standard deviation (0.11 Å) for distances between pairs of atoms, estimated in the preceding section. As expected, the final values are intermediate between SODr_1 and SODr_2. The co-ordination distances in SODr appear longer than in oxidised Cu,Co SOD as expected for Cu(I) co-ordination even if the differences remain in most cases below three standard deviations. However, the overall co-ordination polyhedra in SODr and oxidised SOD are similar. This is in strong contrast with the mechanism proposed by Tainer *et al.* (1983), which involves the breaking of the imidazole bridge formed by His61 between Cu and Zn ions. Figure 12 shows the disposition of the metal ions and their co-ordinating residues.

The metal co-ordination distances are similar between subunits A and subunit B. The largest

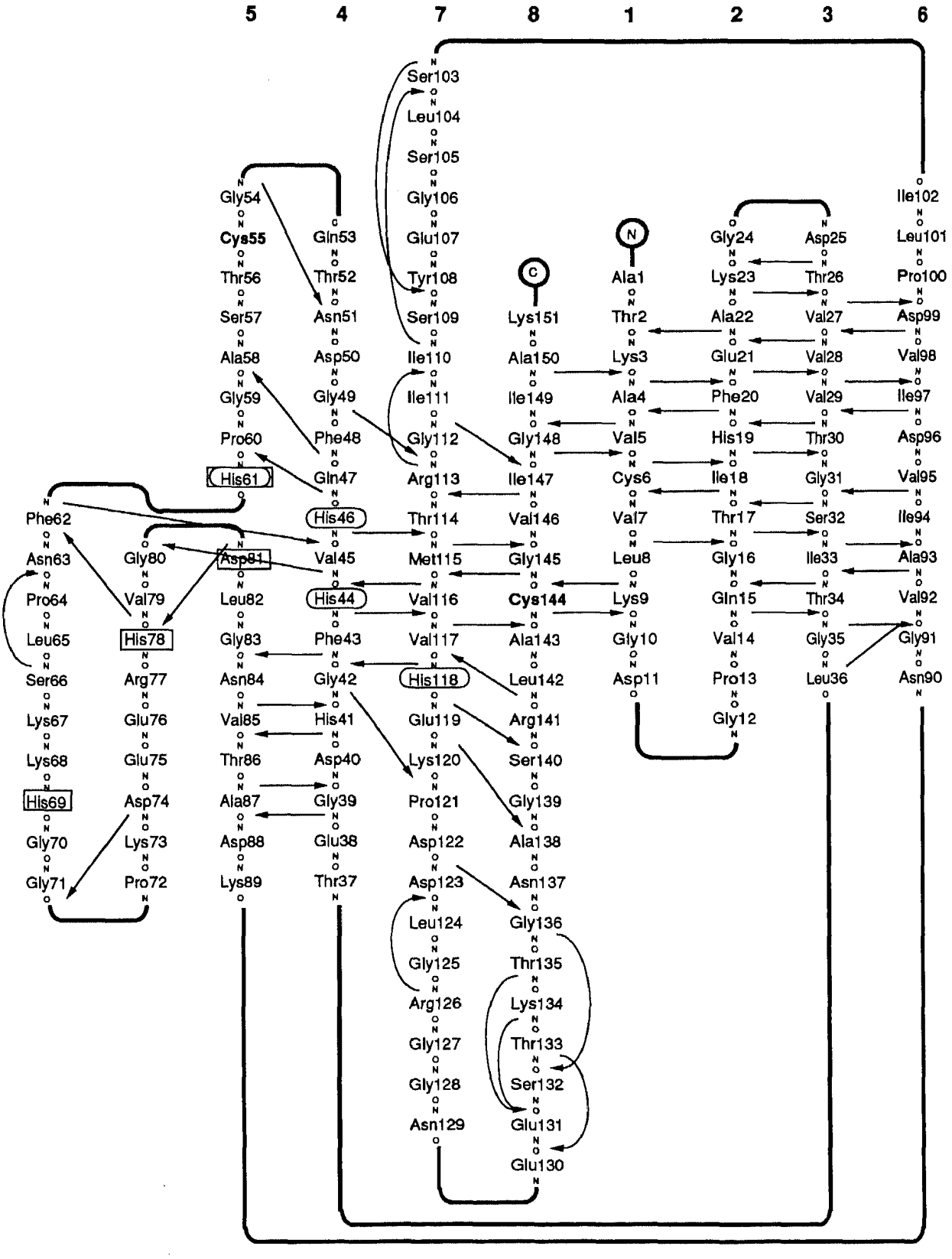

Figure 8. A representation of the topology of a SODr subunit. Main-chain to main-chain hydrogen bonds are represented by arrows. Residues co-ordinating the copper ion are marked with an oval box, residues co-ordinating zinc ion are marked with a rectangular box. Cys55 and Cys144, which form a disulphide bridge are marked with bold type. β-Strands are numbered along the top of the Figure.

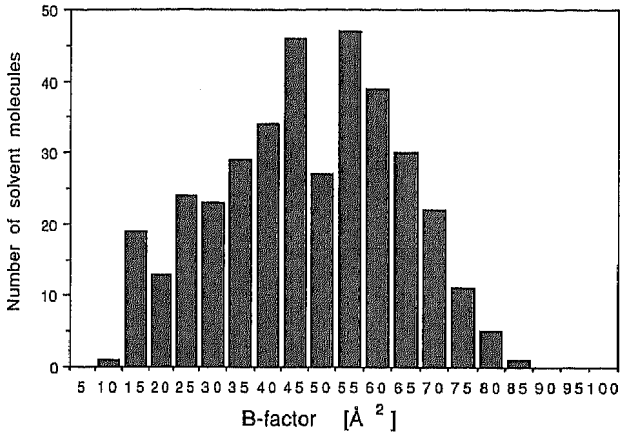

Figure 9. A histogram of the temperature factors for the solvent molecules in the final SODr model.

difference is in the distance between copper and His61. It is almost three standard deviations and could be significant. Larger differences are observed between the co-ordination geometries of the two sites. Copper in site A may be described as being at the centre of a flattened tetrahedron with the water molecule interacting only weakly with it. In site B the copper geometry is better described in terms of a distorted trigonal bipyramid having at the apices His61 and His118 with the other three ligands (His46, His 44 and the water molecule) in the basal plane.

The catalytically important Arg141, Thr35 and Glu131 have conformations similar to those found in the oxidised structure. Lys134, another of the conserved residues, is disordered in both subunits and in the oxidised forms. Contrary to molecular dynamics simulations (Banci *et al.*,1994), Arg141 is well ordered in both subunits and in the oxidised structure. The water structure is significantly different in the two subunits. In subunit B the copper ion is tightly bound to a well defined water molecule while in subunit A the solvent near the Cu ion is not well-defined. The electron density has an elongated shape, which can be interpreted as static or/and dynamic disorder of the water molecules. The closest approach a water molecule, within this density, can make to the copper ion is approximately 3 Å, significantly larger than in subunit B. This tighter binding of ligand to copper is reflected in the lower temperature factor of Cu^+ in subunit B than in subunit A (Table 3). In the model of oxidised Cu,Co SOD (Djinovic *et al.*, 1992) the copper to water distance is also longer in subunit A than in subunit B, by approximately 0.5 Å. The differences in the active centres between subunits A and B extend to other nearby solvent molecules. In general, the solvent in the catalytic site in subunit B is better ordered. In subunit B, solvent molecules form a remarkably well-defined chain filling a groove formed by the catalytic site (Figure 13). A similar pattern of water molecules is seen in the active site in subunit A but the solvent is less ordered. All the well-ordered solvent sites, shown in Figure 13, are found also in the model of oxidised Cu,Co SOD (Djinovic *et al.*, 1992). Djinovic *et al.* (1992) suggested that the solvent sites in the immediate neighbourhood of the active site indicate the successive steps in the diffusion of dioxygen anion to the active site. We suggest that this remarkable structure of water molecules, tightly bound by hydrogen bonds, serves as an efficient relay for delivering protons from the solvent to the bound substrate. An efficient mechanism for delivering the protons to the reaction centre is required to explain the insensitivity of the catalytic rate of SOD to pH changes over the range 5 to 9.5 (Klug *et al.*, 1972). Such a mechanism would also eliminate the requirement for protonated His61 as a proton donor.

Both catalytic sites contain features in the electron density indicating partially disordered solvent. The direction of disordering is always along the direction of the groove, in the vicinity of the conserved Arg141. These features indicate the direction of movement of solvent and probably substrate molecules in the vicinity of the active site.

The differences in the metal co-ordination by water and in the surrounding water structure are clearly

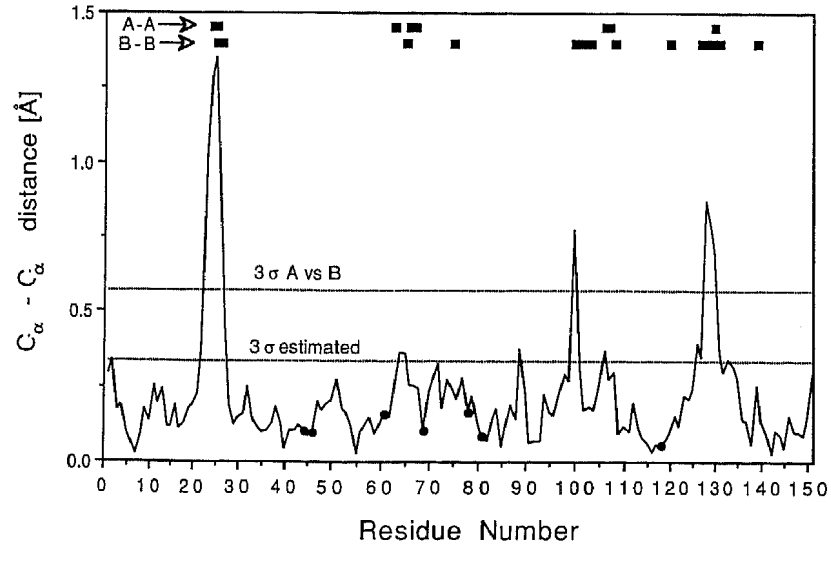

Figure 10. Difference in co-ordinates of α-carbon atoms between subunits A and B, superimposed by least-squares minimisation, as described in the text. Residues participating in intermolecular contacts are indicated along the top of the diagram, separately for the two regions of contact. The upper horizontal line marks the 3σ level as derived from the σ_A plot. The lower horizontal line marks the 3σ level derived from comparing the two independently refined models of SODr.

Table 1. Intermolecular contacts in reduced SOD

Residue	Atom	Atom	Residue	Distance (Å)	Comments
A. *Region 1 (subunit A-subunit A)*					
Gly24	C^{α}	O	Ser66	3.32	
Asp25	N			3.10	H-bond
	$O^{\delta 1}$			3.30	
		C^{α}		3.39	
		C		3.27	
	$O^{\delta 2}$	$N^{\delta 2}$	Asn63	3.03	H-bond
		O	Lys67	3.41	
	C^{γ}			3.34	
Gly106	C^{α}	$O^{\epsilon 1}$	Glu130	3.36	
Glu107	N			2.97	H-bond
B. *Region 2 (subunit B-subunit B)*					
Asp25	O	N	Glu130	3.04	H-bond
		C^{α}		3.10	
		C^{β}		3.10	
Thr26	$O^{\gamma 1}$	$O^{\epsilon 1}$		3.06	H-bond
Pro100	C^{α}			3.41	
	C^{β}			3.38	
	O	N		3.27	H-bond
		N	Glu131	2.92	H-bond
		C^{β}		3.41	
		C^{β}	Asn129	3.40	
Leu101	O			3.25	
		$N^{\delta 2}$		2.96	H-bond
Tyr108	C^{γ}			3.50	
	$C^{\delta 2}$			3.49	
		O	Gly127	3.29	
Leu65	O	C^{ϵ}	Lys120	3.34	
		N^{ζ}		2.87	H-bond
Glu75	$O^{\epsilon 2}$	C^{α}	Gly139	3.36	
Ser103	$O^{\gamma}B^{a}$	O	Gly128	3.07	H-bond

[a] One of two alternative conformations.

significant. One explanation is that they are caused by differences in crystal environment between the subunits. Neither subunit has direct crystal contacts in the neighbourhood of the active site, but in subunit B, Glu75 from a neighbouring molecule makes indirect contact through water molecules in and near the active site. This could cause the observed difference in the solvent structure by stabilising the local solvent structure. The effect of disrupting the electrostatic field near the active site could also be considered. The electrostatic field associated with the active site in SOD is considered to be an important and conserved feature of the enzyme mechanism (Desideri *et al.*, 1992; Sines *et al.*, 1990).

Anisotropic vibrations

A pattern of positive and negative peaks on the $(F_o - F_c)$ difference map near the metal ions shows

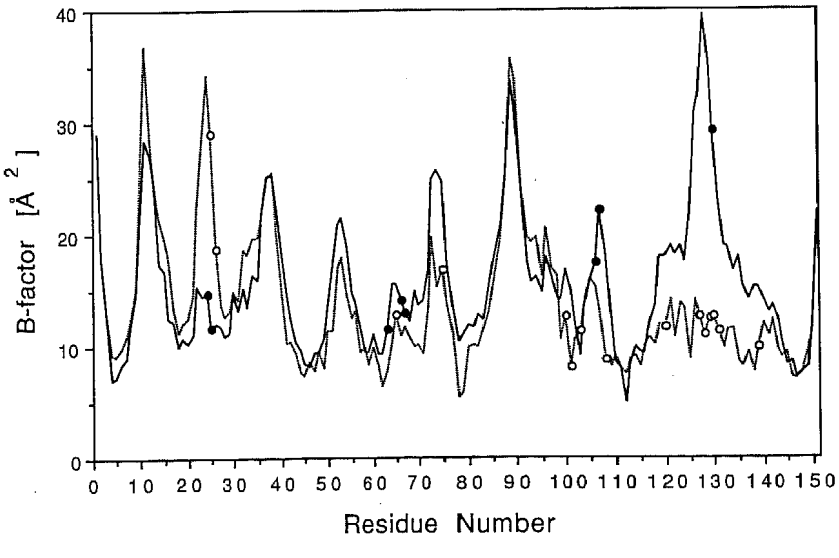

Figure 11. Main-chain temperature factors, averaged for each residue, as a function of residue number, for subunit A (continuous line) and B (broken line). Residues participating in intermolecular contacts are marked with circles.

Table 2. Comparison of the bond distances and angles in the active sites of SOD, for the two independently refined models (SODr_1, SODr_2) and the final model

	Subunit A				Subunit B			
	SODr_1	SODr_2	SODr final	Oxidised SOD (Djinovic *et al.*, 1992)	SODr_1	SODr_2	SODr final	Oxidised SOD (Djinovic *et al.*, 1992)
A. *Comparison of bond distances* (Å)								
Cu^{+}-$N^{\delta 1}$ His44	2.20	2.14	2.16	2.09 (Cu^{2+})	2.12	2.10	2.14	2.02 (Cu^{2+})
Cu^{+}-$N^{\epsilon 2}$ His46	2.23	2.22	2.21	2.29 (Cu^{2+})	2.27	2.24	2.20	2.18 (Cu^{2+})
Cu^{+}-$N^{\epsilon 2}$ His61	2.27	2.37	2.31	2.16 (Cu^{2+})	2.01	2.07	2.02	1.99 (Cu^{2+})
Cu^{+}-$N^{\epsilon 2}$ His118	2.17	2.22	2.19	2.13 (Cu^{2+})	2.10	2.12	2.08	2.14 (Cu^{2+})
Cu^{+}-water	~3	~3	~3	2.89 (Cu^{2+})	2.46	2.64	2.14	2.38 (Cu^{2+})
Zn^{2+}-$N^{\delta 1}$ His61	2.07	2.01	2.03	2.11 (Co^{2+})	2.17	2.07	2.14	1.99 (Co^{2+})
Zn^{2+}-$N^{\delta 1}$ His69	2.25	2.18	2.21	2.01 (Co^{2+})	2.30	2.20	2.24	2.32 (Co^{2+})
Zn^{2+}-$N^{\delta 1}$ His78	2.20	2.15	2.18	2.02 (Co^{2+})	1.91	1.94	1.91	1.97 (Co^{2+})
Zn^{2+}-$N^{\delta 1}$ His81	1.83	1.99	1.89	1.99 (Co^{2+})	1.90	2.05	2.01	1.96 (Co^{2+})
B. *Comparison of angles (degrees)*								
$N^{\delta 1}$ His44-Cu^{+}-$N^{\epsilon 2}$ His46	145.0	142.7	142.5	148.2 (Cu^{2+})	138.9	139.2	137.2	142.1 (Cu^{2+})
$N^{\delta 1}$ His44-Cu^{+}-$N^{\epsilon 2}$ His61	83.5	84.3	85.4	81.7 (Cu^{2+})	88.9	88.8	88.8	79.0 (Cu^{2+})
$N^{\delta 1}$ His61-Cu^{+}-$N^{\epsilon 2}$ His118	96.6	95.6	97.4	95.8 (Cu^{2+})	87.2	87.4	86.8	97.6 (Cu^{2+})
$N^{\epsilon 2}$ His118-Cu^{+}-water	~130	~127	~127	127.0 (Cu^{2+})	128.8	125.3	124.5	121.6 (Cu^{2+})
$N^{\epsilon 2}$ His46-Cu^{+}-$N^{\epsilon 2}$ His61	93.7	92.1	92.8	97.3 (Cu^{2+})	98.4	94.7	93.1	100.2 (Cu^{2+})
$N^{\epsilon 2}$ His46-Cu^{+}-$N^{\epsilon 2}$ His118	98.3	104.0	104.0	100.5 (Cu^{2+})	99.6	97.7	98.0	94.9 (Cu^{2+})
$N^{\epsilon 2}$ His46-Cu^{+}-water	~82	~96	~73	81.5 (Cu^{2+})	91.5	95.3	98.0	94.6 (Cu^{2+})
$N^{\epsilon 2}$ His61-Cu^{+}-$N^{\epsilon 2}$ His118	158.2	152.3	153.3	149.0 (Cu^{2+})	170.1	165.0	167.7	159.5 (Cu^{2+})
$N^{\epsilon 2}$ His61-Cu^{+}-water	75.4	72.3	73.4	73.2 (Cu^{2+})	82.3	81.0	80.1	77.5 (Cu^{2+})
$N^{\epsilon 2}$ His118-Cu^{+}-water	88.2	86.4	84.8	84.5 (Cu^{2+})	93.1	89.4	92.2	87.5 (Cu^{2+})
$N^{\delta 1}$ His61-Zn^{2+}-$N^{\delta 1}$ His69	110.3	111.7	110.9	111.6 (Co^{2+})	108.7	108.7	109.8	107.6 (Co^{2+})
$N^{\delta 1}$ His61-Zn^{2+}-$N^{\delta 1}$ His78	109.1	106.9	108.1	115.2 (Co^{2+})	109.0	107.4	109.1	115.6 (Co^{2+})
$N^{\delta 1}$ His61-Zn^{2+}-$N^{\delta 1}$ Asp81	110.8	109.4	110.1	93.4 (Co^{2+})	102.0	103.5	103.7	94.0 (Co^{2+})
$N^{\delta 1}$ His69-Zn^{2+}-$N^{\delta 1}$ His78	118.9	119.5	119.6	115.3 (Co^{2+})	120.3	122.0	121.5	118.4 (Co^{2+})
$N^{\delta 1}$ His69-Zn^{2+}-$N^{\delta 1}$ Asp81	95.1	96.4	96.1	99.2 (Co^{2+})	92.4	93.8	92.2	94.0 (Co^{2+})
$N^{\delta 1}$ His78-Zn^{2+}-$N^{\delta 1}$ Asp81	112.0	112.6	111.5	119.3 (Co^{2+})	122.2	119.5	118.5	124.0 (Co^{2+})

The distances for the oxidised Cu-Co SOD (Djinovic *et al.*, 1992) are shown for comparison. Only an approximate value can be given for Cu^{+}-water distance in subunit A of reduced SOD. As opposed to subunit B, the water molecule in subunit A is not well defined.

that all four metal ions undergo anisotropic vibrations. In subunit B (Figure 12) both metals vibrate in approximately the same direction, whereas in subunit A the Zn^{2+} has an axis of vibration approximately perpendicular to Cu^{+}. It is difficult to examine the anisotropy in greater detail at this resolution but it is interesting that it can be observed at all. There is no clear correlation between the direction of vibration of the metal ions and the temperature factors of the metal co-ordinating residues.

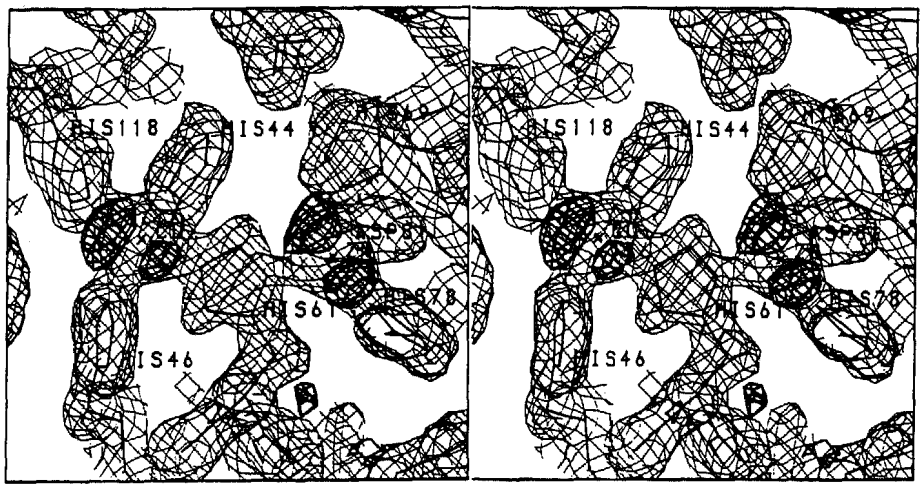

Figure 12. Metal ions and their ligands in reduced SOD, subunit B. The view is from the solvent side. The solvent molecule (not shown) bound to the copper ion is directly above the plane of the paper. Thin contours represent the $(3F_o - 2F_c)$ map at 1σ level. Anisotropic vibrations of the metal ions are seen on the $(F_o - F_c)$ difference map contoured at 3σ (thick contours). Only negative peaks are shown for clarity. The metals vibrate in a direction approximately perpendicular to the plane of the paper.

Table 3. Temperature factors (Å²) of the metal co-ordinating residues and metal ions in reduced SOD

	Subunit A		Subunit B	
	Main-chain average *B* factor (Å²)	Side-chain average *B* factor (Å²)	Main-chain average *B* factor (Å²)	Side-chain average *B* factor (Å²)
His44 (Cu)	10.2	10.7	7.2	11.0
His46 (Cu)	8.2	7.3	8.5	8.0
His118 (Cu)	13.4	13.4	9.8	7.3
His61 (Cu,Zn)	9.5	13.7	7.7	9.5
His69 (Zn)	15.0	13.2	9.5	6.5
His78 (Zn)	10.0	9.6	5.0	7.4
His81 (Zn)	11.3	11.3	10.0	8.4
Cu^{+}	20.6		13.3	
Zn^{2+}	11.3		9.1	

Covalent modification of Glu119

A closer examination of the electron density reveals a feature near one of the C^{ϵ} atoms of Glu119, which indicates a covalent modification of the side-chain. It can be observed in both subunits but in subunit B (Figure 14) the side-chain is better ordered, being near a region of crystal contact. The peak is too close to C^{ϵ} to be a hydrogen-bonded water molecule. The automatic water refining procedure in ARP repeatedly placed water molecules in the peak and subsequently removed them as being too close to the Glu119 C^{ϵ} atom. Meanwhile, the least-squares procedure persistently misplaced the side-chain of Glu119 towards the unaccounted for density. In order to approximately model the extra density we replaced the water molecule at this site with a calcium ion with 0.5 occupancy. This prevented the atom from being removed by ARP and disabled the van der Waal repulsion term, which in PROLSQ is applied only to atoms with full occupancy factors. After further refinement the "probe" atom was 1.9 Å from Glu119 $O^{\epsilon 1}$, 2.9 Å from Ser140 N, 3.4 Å from Ser140 O^{γ} and 2.8 Å from a water molecule. This implies a covalent bond to the Glu119 side-chain and a hydrogen bond, as an acceptor, to N of Ser140, a water molecule and possibly to Ser140 O^{γ}. The refined temperature factor of the probe atom was 20.4 Å². This is comparable with the temperature factor of the adjacent Glu119 $O^{\epsilon 1}$ (30.9 Å²) implying that the extra density corresponds to the approximately ten electrons that were used. Without chemical analysis it is impossible to determine the exact nature of the modification. We investigated the possibility that Glu119 was modified by dithionite, which was used to reduce the active copper ion, by refining the SODr model, containing only protein atoms, against 2 Å data, previously collected on a conventional X-ray source, from the crystal of the oxidised enzyme. After 30 cycles of least-squares refinement, including the automatic solvent addition, the $(F_o - F_c)$ and $(3F_o - 2F_c)$ maps were inspected and found to contain a clear peak at Glu119, in the same position as in the structure of the reduced enzyme. This rules out modification by dithionite. It is likely that the modification took place *in vivo*. This could explain why no other Glu or Asp residue is observed to be modified. One possible modification for Glu119 that is consistent with the electron density map and the deduced hydrogen-bonding pattern is that one of the carboxyl oxygen atoms is replaced by a hydroxylamine group. The proximity of the modifier group of Glu119 to the active site implies that it could have a role in enzyme mechanism. The hydrogen bond

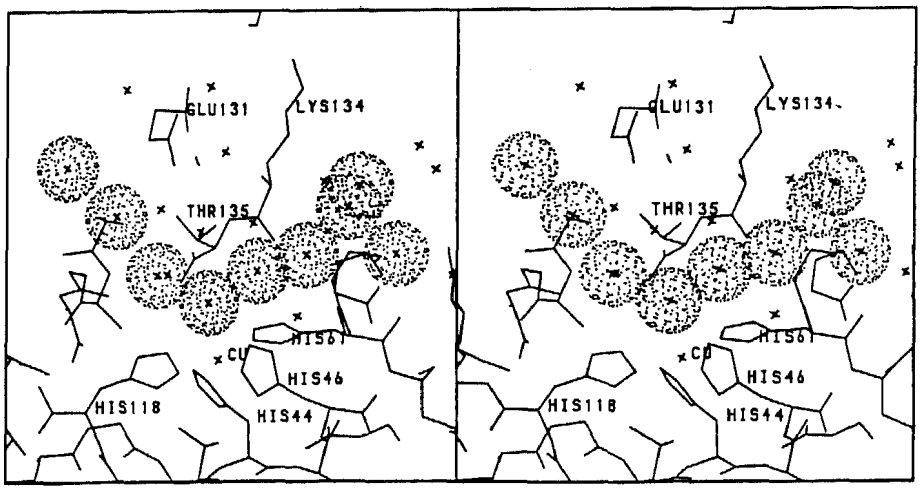

Figure 13. A van der Waals dot surface representation of the chain of solvent molecules filling the groove of the catalytic centre.

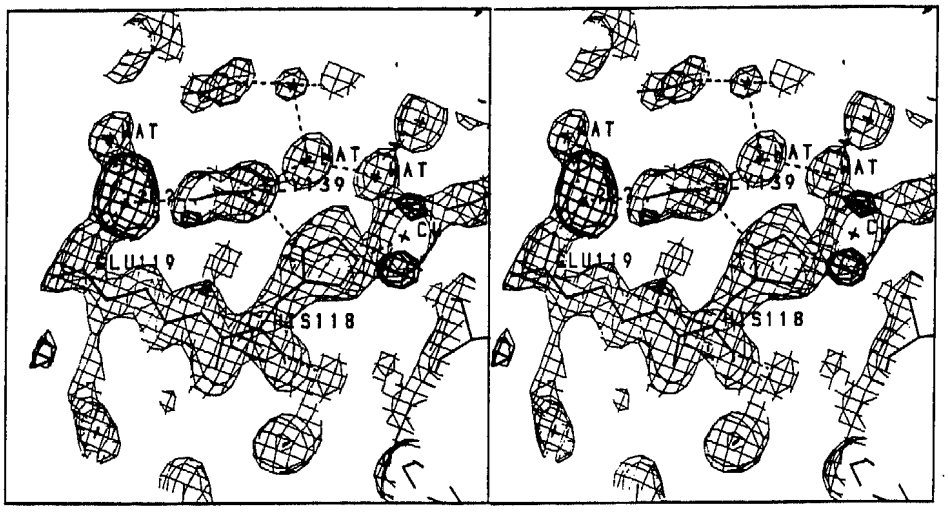

Figure 14. Region of the SODr catalytic site showing chemically modified Glu119. Thin contours represent $(3F_o - 2F_c)$ map at the 1σ level. Thick contours show positive regions of $(F_o - F_c)$ map contoured at 3σ. The maps were calculated with no atom present in the density near Glu119. A dummy atom is shown in the position where previous refinement, with van der Waals repulsion term suppressed, placed a "trial" atom consisting of ten electrons.

to Ser140 N would increase the dipole moment of Ser140 N–Gly139 O. The carbonyl oxygen atom of Gly139 points directly into the active site. It forms a hydrogen bond to a water molecule that is adjacent to the water molecule bound to the copper ion. In the catalytic cycle the negative charge on the carbonyl oxygen atom could propel O_2^- towards the copper ion.

Concluding remarks

SOD crystals diffract at best to a resolution slightly above 2 Å, even in the synchrotron beam. Although the resolution of the diffraction data is the ultimate limitation on the accuracy of the X-ray structures, quality of the data and subsequent analysis can be equally important. We tried to ensure both high quality of the data and accurate error estimates in order to observe small changes in the structure and assess their significance. Obtaining error estimates for the oxidised model would make the two structures more easily comparable.

A still unresolved question is of the different results obtained from the X-ray and spectroscopic data. The two SOD subunits in the crystal provide two independent structural models. Subunit A is fully exposed to the solvent and subunit B is affected by crystal contacts only to a limited extent, through indirect interactions *via* water molecules. In both active sites there is no indication of the imidazole bridge being broken between the Cu and Zn ions. The spectroscopic data also appear to be consistent in showing the bridge being broken in solution. It is likely that the differences between the two models are very small in terms of energy and that both models are relevant to the function of the enzyme. Considering the high turnover rate of SOD, of 10^6 s^{-1} it is unlikely that His61 dissociates at high substrate concentrations (Fee & Bull, 1986). At low substrate concentrations it can dissociate and become protonated but this is not necessary for the catalytic activity. The protons necessary for the reaction can be provided directly by water.

Our results may be reviewed in light of the mechanism for superoxide dismutation by SOD proposed by Osman & Basch (1984). This mechanism is based on quantum mechanical calculations of model systems that show that the complex between Cu(II) and superoxide is indeed very stable, hence the authors propose that the copper reduction may occur through an outer sphere electron transfer between the Cu(II)-O_2^- complex and a second superoxide molecule. This mechanism does not imply the breaking of the His61 bridge as proposed previously (Tainer *et al.*, 1983) and the proton(s) needed by the reaction are not provided by His61.

The structure factors and atomic co-ordinates for SODr_1, SODr_2 and the final model have been deposited with the Protein Data Bank (Bernstein *et al.*, 1977), from which copies may be obtained. The PDB codes are 1SXA for SODr_1, 1SXB for SODr_2 and 1SXC for the final model.

Materials and Methods

Crystal growth

Crystals of Cu(I) bovine erythrocyte superoxide dismutase were grown by slow diffusion of the precipitant solution (16% (w/v) PEG6000 in Tris-HCl buffer at pH 7.5) into the protein solution (8 mg/ml in Tris-HCl buffer, pH 7.5) already reduced by the addition of an excess of sodium dithionite under nitrogen atmosphere. The crystallisation vial was maintained under inert atmosphere throughout the process of crystal growth. Once grown the crystals were stable to reoxidation for four to six weeks.

EPR spectroscopy

EPR data were taken on a Bruker ER200-SRDD spectrometer operating at X-band (ν = 9.78 GHz). The external

magnetic field Ho was calibrated using a DPPH powder sample (g(dpph) = 2.0036). The spectra were collected at room temperature either on single or multiple crystals of Cu(I) superoxide dismutase (SOD) sealed in capillary tubes. For comparison, spectra of single and multiple crystals of Cu(II) SOD and of the capillary tube alone were collected. The spectra of single crystals of the oxidised enzyme evidenced the signal of the paramagnetic Cu(II) ion, whereas the crystals used for crystallographic data collection, having dimensions similar to the oxidised crystal, did not show any EPR signal (Figure 15). The same results were obtained when we used several crystals of Cu(I) SOD from the same batch as that used for the crystallographic data collection (Figure 16). These results show that the amount of oxidised enzyme present in the Cu(I) SOD crystal was below the limit of instrumental sensitivity.

Crystallographic data collection and processing

The crystals belong to space group $P2_12_12_1$ with a = 47.8 Å, b = 51.1 Å, c = 148.0 Å. Diffraction intensities were measured on the EMBL X31 beam line at the DORIS storage ring, DESY, Hamburg, with an imaging plate scanner built at EMBL (J. Hendrix and A. Lentfer, unpublished results). Two separate data sets, denoted SODr_1 and SODr_2, were collected from two different crystals. SODr_2 was recorded to confirm the structural results obtained from SODr_1. Both crystals were mounted with the b^* axis approximately parallel with the spindle axis. The oscillation angle was varied between 0.5° and 1.5° to minimise the overlapping of reflections. The integrated intensities were measured using the program DENZO, version 0.47, and scaled using program SCALEPACK from the DENZO suite (Otwinowski, 1993). Relative temperature factors for images were refined. Adjacent partially recorded reflections were added. Outliers were rejected based on the chi-square test implemented in DENZO. The postrefinement option of SCALEPACK was used to refine the cell parameters. This gave slightly different results for the two data sets (Table 4). The intensities were converted to structure factor amplitudes and a correction was applied to weak or negative measurements based on the *a priori* distribution (French & Wilson, 1978).

The final data set was obtained by scaling together all individual images from both SODr_1 and SODr_2. The merged data contained 28,240 unique reflections and was 97.0% compete to 1.9 Å resolution. The merging R-factor was 10.0%, higher than either of the original data sets. This may reflect small differences between the two crystals from which SODr_1 and SODr_2 data were collected but most probably it reflects the undesirable property of the merging R-factor, which tends to rise as more data are included. Although both SODr_1 and SODr_2 data sets are of high quality, the final, merged data is overall more reliable by having greater redundancy, which should reduce systematic errors, and slightly greater completeness than the constituent data sets. The final postrefined cell parameters were a = 47.8 Å, b = 51.1 Å, c = 148.0 Å. Data collection and reduction for the two constituent data sets and the final, merged data set are summarised in Table 1. The Wilson (1942) plots for SODr_1, SODr_2 and the final, merged data set were very similar. Only the plot for the final data is shown in Figure 17. The fit to the theoretical straight line is satisfactory with the expected deviations for

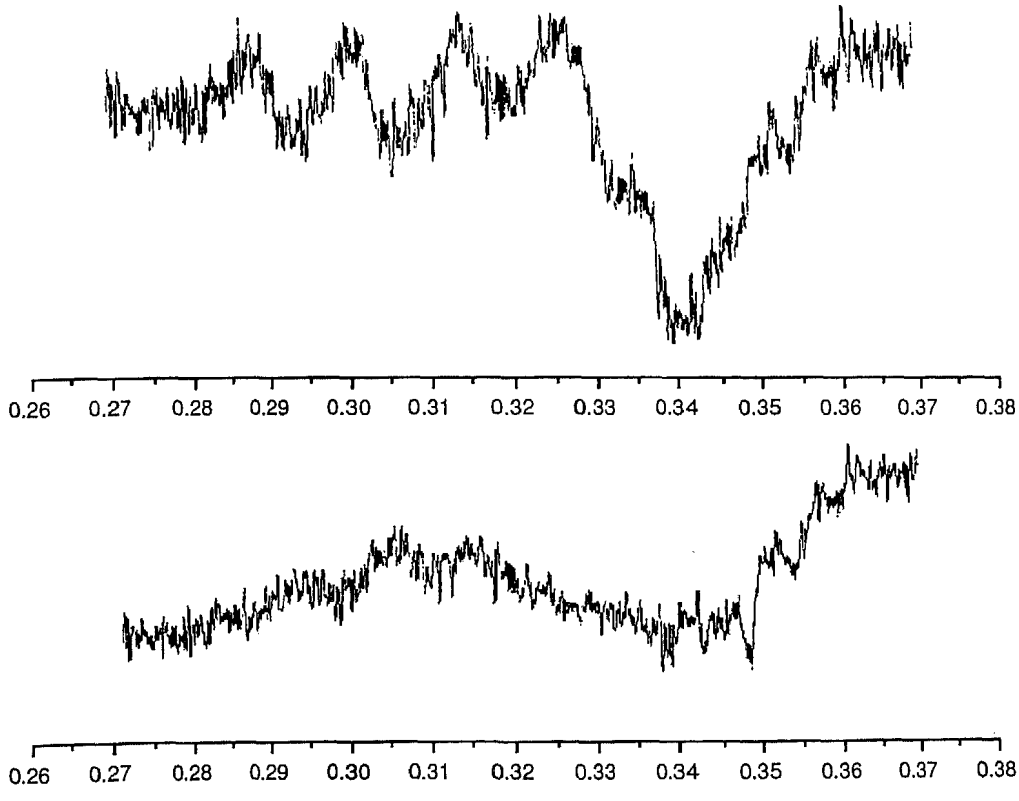

Figure 15. (a) EPR spectrum of a single crystal of Cu(II),Zn SOD compared with (b) the spectrum of the crystal of Cu(I),Zn SOD that had been used in X-ray data collection (SODr_2 data set). The two spectra were recorded with identical instrumental settings (50 scans each). The crystals had similar size. The EPR lines characteristic of Cu(II),Zn SOD, evident in (a) do not appear in (b).

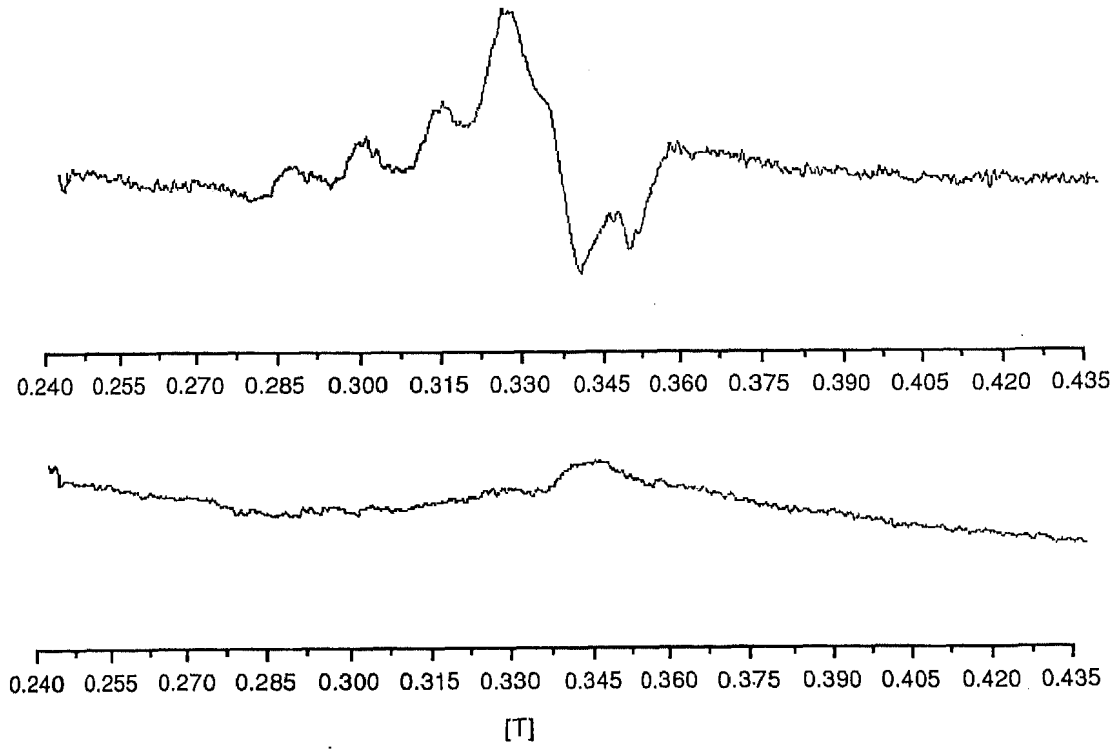

Figure 16. Comparison of EPR spectra of (a) crystalline Cu(II),Zn SOD. (five crystals, approximate volume 4×10^{-3} mm^3 each) with that of (b) the same amount of Cu(I),Zn SOD crystals collected with identical experimental set-up. Each spectrum is a sum of ten scans. The crystals of the reduced enzyme are from the same batch as the crystal used in the X-ray data collection (SODr_1).

a protein in the low-resolution range. The overall temperature factor estimated from the Wilson plot is 24.3 Å^2.

Refinement

Refinement of atomic co-ordinates and temperature factors was carried out by stereochemically restrained least-squares minimisation (Konnert, 1976; Konnert & Hendrickson, 1980) incorporated in the CCP4 program suite (Collaborative Computational Project, Number 4, 1994). The structure of the cobalt-substituted, oxidised form of SOD (Djinovic *et al.*, 1992; PDB code 1COB) was used as the starting model. A low-resolution cut-off of 10 Å was used. No σ cut-off was applied to amplitudes. The weighting parameters for the refinement are listed in Table 5. The co-ordination distances for the metal ions were refined unrestrained. Manual rebuilding of the model was based on $(3F_o - 2F_c)$ and $(F_o - F_c)$ maps, using an Evans and Sutherland ESV graphics station and the program FRODO (Jones, 1978). Solvent molecules were inserted and refined

Table 4. Summary of data

	SODr_1		SODr_2		SODr final (merged SODR_1 and SODR_2)
	High	Low	High	Low	
Maximum resolution (Å)	1.9	3.0	2.0	3.5	1.9
Crystal to plate-distance (mm)	190	350	220	400	—
Oscillation per image (deg.)	0.5–1.5	1.0–3.0	0.75–1.5	1.5–4.0	—
Number of exposures	105	55	90	39	294
Approx. time/exposure (s)	300	30	360	60	—
Wavelength (Å)	0.97				
% $R_{merge}(I)$[a]	7.3		7.0		10.0
Raw measuments used	136,349		123,022		259,693
Unique reflections	26,203		24,927		28,240
% Completeness (excl. ∞–10.0 Å)	90.5		98.0		97.0
% Greater than 3σ	82		86		86
Post-refined cell param. (Å)					
a	47.9		47.7		47.8
b	51.1		51.0		51.1
c	148.2		147.8		148.0

[a] $R_{merge}(I) = \Sigma|I_i - \langle I\rangle|/\Sigma\langle I\rangle$, where I_i is an individual intensity measument, and $\langle I\rangle$ is the average intensity for this reflection. The summation is over all data.

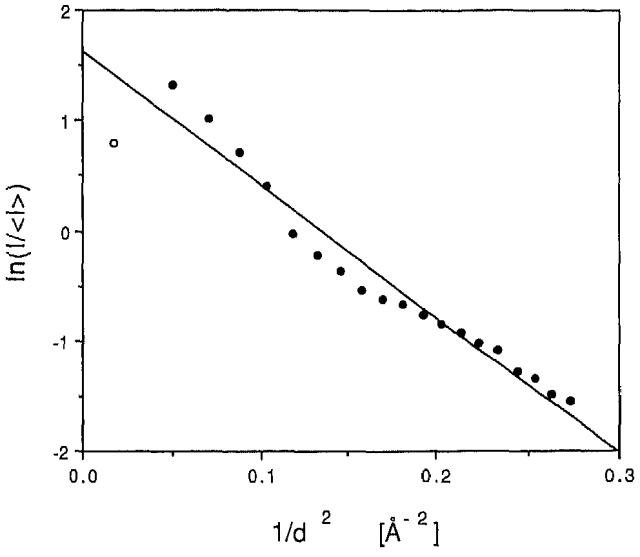

Figure 17. Wilson plot for the final SODr data set. The linear correlation coefficient is 0.96, after omitting the most outlying point (void symbol) in the lowest resolution range.

using the program ARP (Lamzin & Wilson, 1993), an automatic procedure of peak search with distance constraints, real space fitting, density shape analysis, merging of atoms and automatic determination of statistically significant density level for defining new water molecule sites (ARP, version 4.0, Lamzin & Wilson, unpublished). ARP was set up to remove water molecules from the model if they were found in density less than 0.5σ in the $(3F_o - 2F_c)$ map. The option for automatic determination of statistically significant density level relies on estimating the underlying normal distribution of the electron density and comparing it with the observed distribution in the $(F_o - F_c)$ map. The threshold level of significant density determined by the program was approximately constant throughout the refinement, close to the 4σ level in the $(F_o - F_c)$ map. Potential new water molecule sites had to be within 2.2 to 3.3 Å of existing atoms in the model to be considered. Water molecules were merged into a single site if the distance between them became less than 2.2 Å. All solvent molecules were refined with occupancy factor set to 1. Initially, 35 cycles of least-squares refinement were performed on each model, interspersed with five rounds of manual rebuilding. This was followed by 30 more cycles of the ARP procedure to refine the water structure. The final *R*-factors were 16.6% and 15.3% for SODr_1 and SODr_2, respectively. Several disordered side-chains, or parts of side-chains, were omitted from the model by setting the atomic occupancy factors to 0. These were the side-chains of lysine 3, 9, 23, 68, 73, 89, 120, 134 and 151, Gln53, Asp75 and Glu107 from subunit A, and lysine 9, 23, 73, 89 and 134, Asn51 and Gln53 from subunit B. The two models contained 2136 protein atoms and four metal ions each. SODr_1 contained 299 water molecules and SODr_2 contained 349 water molecules.

Refinement against the final, merged data set proceeded as follows. The model obtained from SODr_1 was taken as the starting model and refined initially for 20 least-squares cycles, including the automatic solvent refinement protocol, as described above, and three rounds of manual inspection and rebuilding. A further 30 cycles were run to refine the water structure with ARP. The final *R*-factor for the model was 15.6%. The final model contains 2156 protein atoms, four metal ions and 371 solvent molecules. The statistics for stereochemistry and temperature factors is summarised in Table 5. Some side-chain atoms that were omitted as disordered from the SODr_1 and SODr_2 models could now be seen (Glu53 and Asp75 from subunit A and Lys9 from subunit B). The final $(F_o - F_c)$ map had r.m.s. 0.06 e/Å^3, with maximum of 0.9 e/Å^3 and minimum −0.3 e/Å^3.

Acknowledgements

We thank Zbigniew Dauter for helpful discussion.

Table 5. Weighting parameters for the least-squares refinement and the final standard deviations

	σ[a]	Standard deviation	Number of parameters
A. *Distances (Å)*			
Bond lengths (1-2 neighbours)	0.020	0.015	2190
Bond angles (1-3 neighbours)	0.040	0.038	2971
Dihedral angles (1-4 neighbours)	0.050	0.048	710
Planar groups	0.020	0.014	392
Chiral volumes	0.200	0.183	340
B. *Non-bonded contacts (Å)*			
Single torsion	0.500	0.19	795
Multiple torsion	0.500	0.35	836
Possible hydrogen-bonding contacts	0.500	0.24	193
C. *Torsion angles (deg.)*			
Peptide plane (ω)	5.0	2.6	308
Staggered (aliphatic χ_1)	15.0	12.6	340
Orthonormal (aromatic χ_2)	20.0	36.7	26
D. *Thermal factors (Å^2)*			
Main-chain bond	3.0	2.27	1274
Main-chain angle	4.0	3.10	1596
Side-chain bond	4.0	4.75	916
Side-chain angle	5.0	6.96	1375

[a] The weights correspond to $1/\sigma^2$.

References

Azab, H. A., Banci, L., Borsari, M., Luchinat C., Sola, M. & Viezzoli, M. S. (1992). Redox chemistry of superoxide dismutase. Cyclic voltammetry of wild-type enzymes and mutants on functionally relevant issues. *Inorg. Chem.* **31**, 4649–4655.

Banci, L., Bertini, I., Bruni, B., Carloni, P., Luchinat, C., Mangani, S., Orioli, P. L., Piccioli, M., Rypniewski, W. & Wilson, K. S. (1994). X-ray, NMR and molecular dynamics studies on reduced bovine superoxide dismutase: implications for the mechanism. *Biochem. Biophys. Res. Commun.* **202**, 1088–1095.

Bernstein, F. C., Koetzle, T. F., Williams, G. J. B., Meyer, E. F. Jr, Brice, M. D., Rodgers, J. R., Kennard, O., Shomanouchi, T. & Tasumi, M. (1977). The protein data bank: a computer-based archival file for macromolecular studies. *J. Mol. Biol.* **112**, 535–542.

Bertini, I., Luchinat, C. & Monnanni, R. (1985). Evidence of the breaking of the copper-imidazole bridge in copper/cobalt-substituted superoxide dismutase upon reduction of the Cu(II) centers. *J. Am. Chem. Soc.* **107**, 2178–2179.

Bertini, I., Banci, L., Luchinat, C. & Piccioli, M. (1990). Spectroscopic studies on Cu_2Zn_2SOD: a continuous advancement of investigation tools. *Coord. Chem. Rev.* **100**, 67–103.

Bertini, I., Capozzi, F., Luchinat, C., Piccioli, M. & Viezzoli, M. S. (1991). Assignment of active site protons in the ^{1}H NMR spectrum of reduced human Cu,Zn superoxide dismutase. *Eur. J. Biochem.* **197**, 691–697.

Blackburn, N. J., Hasnain, S. S., Binsted, N., Diakun, G. P., Garner, C. D. & Knowles, P. F. (1984). An extended-X-ray-absorption-fine-structure study of bovine erythrocyte superoxide dismutase in aqueous solution. *Biochem. J.* **219**, 985–990.

Collaborative Computational Project, Number 4 (1994). The CCP4 suite: programs for protein crystallography. *Acta Crystallog. sect. D*, **50**, 760–763.

Desideri, A., Felconi, M., Polticelli, F., Bolognesi, M., Djinovic, K. & Rotillo, G. (1992). Evolutionary conservativeness of electrostatic field in the Cu,Zn superoxide dismutase active site. *J. Mol. Biol*, **223**, 332–352.

Djinovic, K., Coda, A., Antollini, L., Pelosi, G., Desideri, A., Falconi, M., Rotilio, G. & Bolognesi, M. (1992). Crystal structure solution and refinement of the semi-synthetic cobalt-substituted bovine erythrocyte superoxide dismutase at 2.0 Å resolution. *J. Mol. Biol.* **226**, 227–238.

Fee, J. A. & Bull, C. (1986). Steady-state kinetic studies of superoxide dismutases. *J. Biol. Chem.* **261**, 13000–13005.

French, S. & Wilson, K. S. (1978). On treatment of negative intensity observations. *Acta Crystallog. sect. A*, **34**, 517–525.

Fridovich, I. (1975). Superoxide dismutase. *Annu. Rev. Biochem.* **44**, 147–159.

Jones, T. A. (1978). A graphics model building and refinement system for macromolecules. *J. Appl. Crystallog.* **11**, 268–272.

Klug, D., Rabani, J. & Fridovich, I. (1972). A direct demonstration of the catalytic action of bovine erythrocyte superoxide dismutase through the use of pulse radiolysis. *J. Biol. Chem.* **247**, 4839–4842.

Konnert, J. H. (1976). A restrained-parameter structure-factor least-squares refinement procedure for large asymmetric units. *Acta Crystallog. sect. A*, **32**, 614–617.

Konnert, J. H. & Hendrickson, W. A. (1980). A restrained-parameter thermal-factor refinement procedure. *Acta Crystallog. sect. A*, **36**, 344–350.

Kraulis, P. J. (1991). MOLSCRIPT: a program to produce both detailed and schematic plot of protein structures. *J. Appl. Crystallog.* **24**, 946–960.

Lamzin, V. S. & Wilson, K. S. (1993). Automated refinement of protein models. *Acta Crystallog. sect. D*, **49**, 129–147.

Luzzati. V. (1952). Traitement statistique des erreurs dans la determination des structures cristallines. *Acta Crystallog.* **5**, 802–810.

McAdam, M. E., Fielden, E. M., Lavelle, F., Calabrese, L., Cocco, D. & Rotilio, G. (1977). The involvement of the bridging imidazole in the catalytic mechanism of the action of bovine superoxide dismutase, *Biochem. J.* **167**, 271–274.

Osman, R. & Basch, H. (1984). On the mechanism of superoxide dismutase: a theoretical study. *J. Am. Chem. Soc.* **106**, 5710–5714.

Otwinowski, Z. (1993). Oscillation data reduction program. In *Proceedings of the CCP4 Study Weekend. Data Collection and Processing*, pp. 56–62. SERC Daresbury Laboratory, Warrington.

Read, R. J. (1986). Improved Fourier coefficients for maps using phases from partial structures with errors. *Acta Crystallog. sect. A*, **42**, 140–149.

Rotilio, G., Finazzi, Agró, A., Calabrese, L., Bossa, F., Guerrieri, P. & Mondoví, B. (1971). Metal sites of copper proteins. Ligands of copper in hemocuprein. *Biochemistry*, **10**, 616–621.

Sines, J. J., Allison, A. A., McCamenon, J. A. (1990). Point charge distribution of end electrostatic steering in enigma/substrate encounter: brownian dynamics of modified copper/zinc superoxide dismutases. *Biochemistry*, **20**, 9403–9412.

Tainer, J. A., Getzoff, E. D., Beem, K. M., Richardson, J. S. & Richardson, D. C. (1982). Determination and analysis of 2 Å structure of copper zinc superoxide dismutase. *J. Mol. Biol.* **160**, 181–217.

Tainer, J. A., Getzoff, E. D., Richardson, J. S. & Richardson, D. C. (1983). Structure and mechanism of copper, zinc superoxide dismutase, *Nature*, **306**, 284–287.

Valentine, J. S. & Pantoliano, M. W. (1981). Protein-metal ion interactions in cuprozinc proteins, In *Metal Ions in Biological Systems* (Sigel, H., ed.), Vol. 3, pp. 291–358, Dekker, New York.

Wilson, A. J. C. (1942). Determination of absolute from relative X-ray data intensities. *Nature*, **150**, 151–152.

Edited by T. Richmond

(Received 20 December 1994; accepted in revised form 2 June 1994)